



Numerical investigation of ice accretion on an offshore composite wind turbine under critical loads

Oumnia Lagdani, Mostapha Tarfaoui, Mourad Nachtane, Mourad Trihi,
Houda Laaouidi

► To cite this version:

Oumnia Lagdani, Mostapha Tarfaoui, Mourad Nachtane, Mourad Trihi, Houda Laaouidi. Numerical investigation of ice accretion on an offshore composite wind turbine under critical loads. International Journal of Energy Research, 2021, 45 (3), pp.4112-4132. 10.1002/er.6073 . hal-03028504

HAL Id: hal-03028504

<https://ensta-bretagne.hal.science/hal-03028504>

Submitted on 25 Jun 2021

HAL is a multi-disciplinary open access archive for the deposit and dissemination of scientific research documents, whether they are published or not. The documents may come from teaching and research institutions in France or abroad, or from public or private research centers.

L'archive ouverte pluridisciplinaire **HAL**, est destinée au dépôt et à la diffusion de documents scientifiques de niveau recherche, publiés ou non, émanant des établissements d'enseignement et de recherche français ou étrangers, des laboratoires publics ou privés.

Numerical investigation of ice accretion on an offshore composite wind turbine under critical loads

Oumnia Lagdani¹  | Mostapha Tarfaoui² | Mourad Nachtane³ |
Mourad Trihi¹ | Houda Laaouidi¹

¹Laboratory for Renewable Energy and
Dynamic Systems, FSAC—UH2C,
Morocco

²ENSTA Bretagne, IRDL UMR CNRS
6027, Brest, France

³Arts et Metiers Institute of Technology,
Bordeaux INP, INRAE, I2M Bordeaux,
University of Bordeaux, CNRS, Talence,
France

In northern regions, wind turbines are affected by the formation of ice on the surface of their structures, which usually occurs on moving blades, resulting in a significant decrease in aerodynamic performance and then the output power tends to reduce. This research evaluates the mechanical behavior and damage of the proposed composite blade structure under icing conditions. A comparative evaluation was carried out considering three ice configurations and three blade positions. The results are then examined and analysed. During this study, the blade in service was subjected to three different critical loads. A numerical simulation is adopted using finite element method (FEM) with ABAQUS software to localize damage in the composite wind turbine blade. The method developed is based on the failure criteria of HASHIN to detect failure modes in large structures and to identify the most sensitive zones. Major damage appeared in the transition region and was the principal reason for the composite blade failure. Furthermore, greater strength and stiffness were found with Carbon (CC) fibers blade designs, whereas configuration 3 was found to be the best one, and the optimal blade position was when the ice structure was placed vertically.

KEYWORDS

cold climate, composite materials, finite element analysis, Hashin criterion, ice accretion, wind turbine blade

1 | INTRODUCTION

The increase in the worldwide energy supply of primary energy, pollution, global warming have become priority problems which humanity has addressed. Increasing global primary energy supply and greenhouse gas emissions have become priority challenges confronting us today and must be faced by humanity. However, it is necessary to take stock of the development of renewable energies, which represent a perfect solution and an alternative to fossil fuels.^{1,2} Wind energy is a promising and economical renewable source of energy capable of

generating electricity, which has increased considerably since the 90s. It uses only the force of the wind, has no negative effect on the environment and is endless.^{3,4}

As in all cold climate regions, the winter period is the season when the winds are generally stronger and the air density is the highest.⁵ It is also during this period that electricity consumption peaks are observed, peaks for which the electrical network must call on all the modes of production that can be provided (nuclear, thermal, hydraulic) and even sometimes at imports. In most of the Polar Regions where the cold is severe all year round, without summer heat (10°C maximum) and with freezing

winters, the conditions are perfectly excellent for the exploitation of wind energy.⁶

Wind turbines placed in cold climate countries tend to randomly accumulate ice on their surfaces, Figure 1A; this accretion can take place in different ways even if the turbines are located on the same site. Several problems are directly related to this phenomenon mainly affects various aspects. Accumulated ice can come off the blades of wind turbines, as shown in Figure 1B, causing several damages, which result in high noise emission levels. This noise represents a major obstacle that causes production stoppages with regard to the health of the public living around the wind farms.⁷ The presence of ice alters the aerodynamic shape of the blades and forms attachments to their surfaces which has adverse impacts on the performance and good functioning of wind turbines. The severity of icing at different places on the blade as well as its non-uniform distribution can increase drag, decrease lift and generate excessive vibration problems due to the irregular icing of the blade.⁸ Cold weather is an important factor in design, analysis, and performance tests of wind turbines.⁹ It is essential to provide insight into the behaviour of ice and the damage associated with its shedding problems as well as the behaviour of thermoplastic composites in northern conditions.

H. Farid et al.¹⁰ proposed an empirical failure criterion for atmospheric ice based on experimental observations to determine the behaviour of atmospheric ice in compression and tension, taking into account several parameters. The results obtained showed a good correlation between the experimental data and the values obtained using the failure criterion. The same authors¹¹ evaluated a study of the compressive strength of atmospheric ice under different experimental conditions. Ice

was accumulated in the wind tunnel in a closed loop. The results obtained show a strong dependence of the compressive strength on temperature, strain rate and porosity. Soroush HA Fini et al.¹² studied the elastic deformation of wood-plastic composites (WPC) and HDPE at cold temperatures using the bubble inflation technique. Results from experiments with HDPE and WPC membranes showed that they are elastic in response to pressure at cold temperatures and that the addition of wood fibres to the raw HDPE results in less deformation under pressure and this contribution is greater as the temperature decreases.

Another study carried out by the same authors¹³ to develop a unique approach that uses the results of computer simulations in Abaqus, a finite element package, combined with artificial neural networks is applied in order to find the optimum material constants for different materials at cold temperatures. It was observed that the addition of wood fiber in raw HDPE leads to higher Young's modulus, and thus the material has less deformation under the pressure.

The formation of ice on various components of the wind turbine using composite materials such as carbon

TABLE 1 Blade turbine characteristics

Length of the blade (m)	48
Maximum chord (mm)	3932
Position twists maximum (mm)	R9000
Fluid speed upstream of the blade (m/s)	25
Angular velocity (rpm)	15.7
Frequency of solicitation: Fr (Hz)	0.2

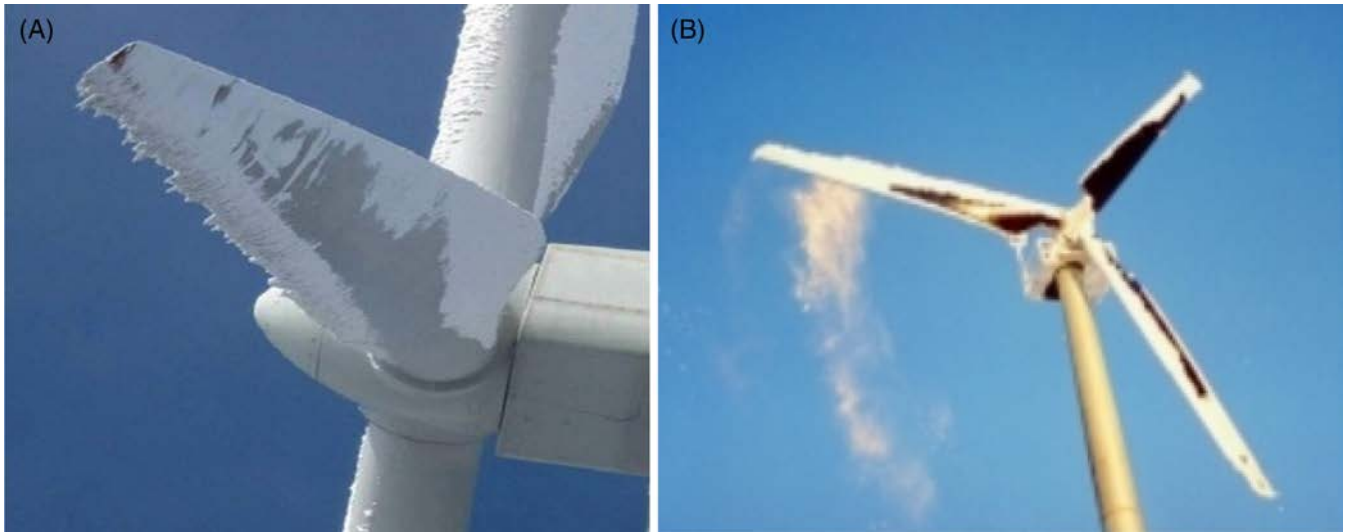


FIGURE 1 Ice accretion on wind turbine blades [Colour figure can be viewed at wileyonlinelibrary.com]

and glass fibers will modify their mechanical properties. These materials are the most commonly used because they are lightweight, due to the uneven shrinkage of their fiber/matrix components, will be subject to residual stress, which can induce premature micro-cracks in the material, causing visible impact damage.¹⁴

According to the literature, many works have been published on the icing of wind turbines. Pedersen and Sorensen¹⁵ modelled ice accumulation and analyzed the aerodynamic performance of the NACA-64618 blade profile using the CFD Computational Fluid method utilizing

the ANSYS-FLUENT software. The blade was exposed to icing conditions for 20 minutes. The experimental analysis revealed that ice accumulates at the leading edge and its mass is increased for higher wind speeds. It was also found that the blade tip is the most susceptible zone for ice accumulation where maximum relative wind speed is reached. Gantasala et al.¹⁶ were interested in assessing the influence of symmetrical and asymmetrical icing at distinct places of the wind turbine blade. They found that half of the total power was produced from the outside third of the blade and that severe icing in this zone will cause a loss of power. The authors also added that

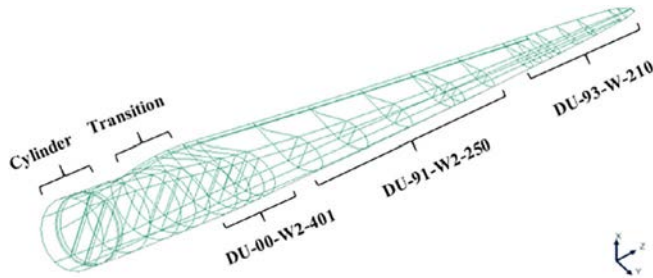


FIGURE 2 Distribution of airfoils throughout the wind turbine blade [Colour figure can be viewed at wileyonlinelibrary.com]

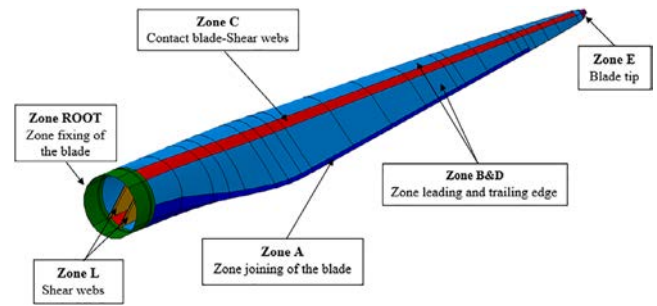


FIGURE 4 Illustration of the different zones of the blade [Colour figure can be viewed at wileyonlinelibrary.com]

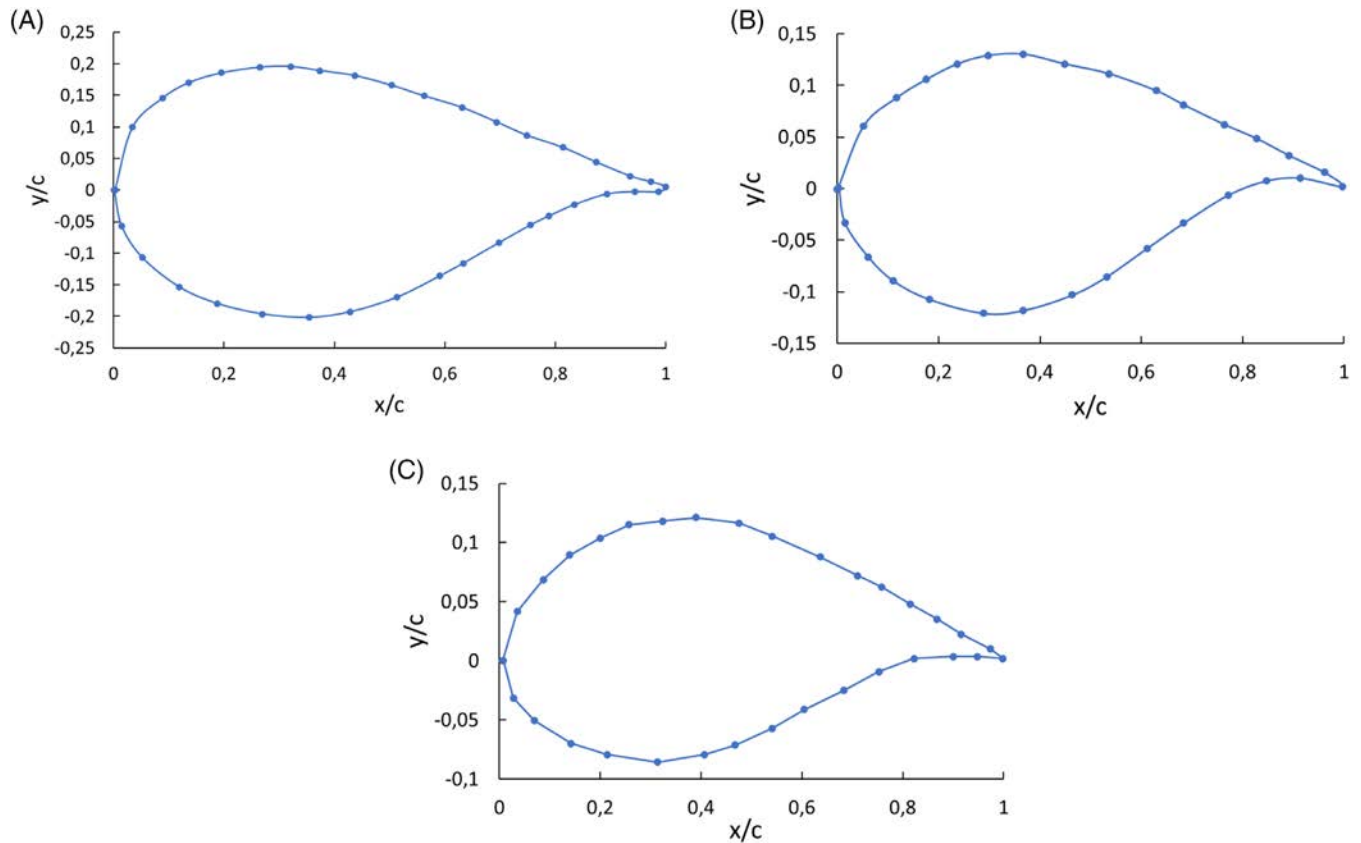


FIGURE 3 Airfoils selected for our offshore wind turbine blade [Colour figure can be viewed at wileyonlinelibrary.com]

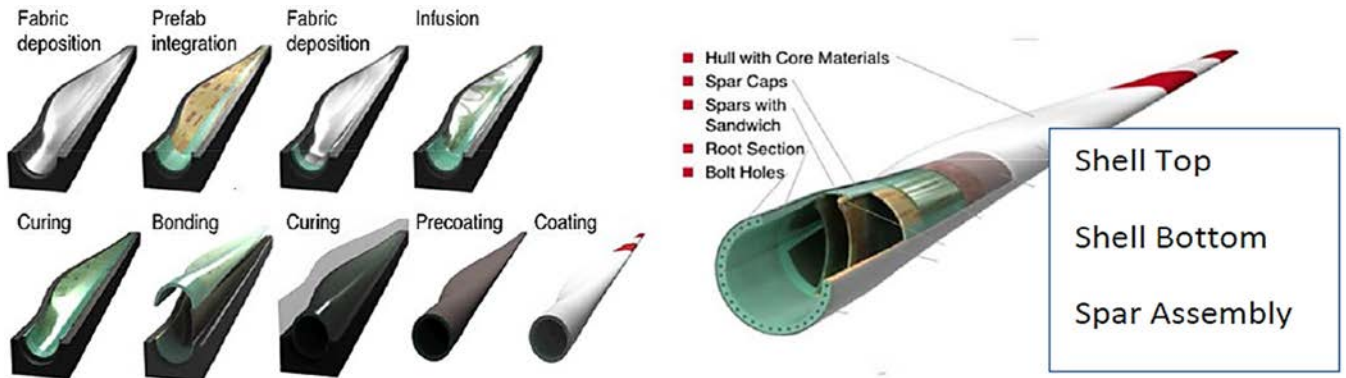


FIGURE 5 Manufacture of a composite blade [Colour figure can be viewed at wileyonlinelibrary.com]

TABLE 2 Properties of composite materials

Properties		Glass-polyester ²⁹	Carbon-epoxy ³²
Physical properties			
Density (kg/m ³)		1960	1600
Engineering constants			
Longitudinal modulus (GPa)	E_1	48.16	147
Transverse modulus (GPa)	$E_2 = E_3$	10.30	10.30
Shearing modulus (GPa)			
$G_{12} = G_{13}$		4.42	7
G_{23}		9	3.7
Poisson's ratio			
$\nu_{12} = \nu_{13}$		0.270	0.27
ν_{23}		0.096	0.54
Strength properties			
Longitudinal tensile (MPa): X_t		1021	2041
Longitudinal compression (MPa): X_c		978	1784
Transverse tensile (MPa): Y_t		29.5	58.7
Transverse compression (MPa): Y_c		171.8	24.78
Shear (MPa): $S_t = S_c$		35.3	65.6
Fracture energies			
Longitudinal tensile (kJ/m ²): G_f^{ft}		200	300
Longitudinal compression (kJ/m ²): G_f^{fc}		500	600
Transverse tensile (kJ/m ²): G_f^{mt}		500	600
Transverse compression (kJ/m ²): G_f^{mc}		500	600

uniform symmetrical icing on all three blades will reduce loads and vibrations as opposed to asymmetrical icing, which creates structural instability and causes loads and vibrations on the tower, hub and nacelle. Hu et al.¹⁷ reported that the mass and thickness of the ice increases linearly from the root to the tip of the blade and is 5 times greater in that area. They also mentioned that the pitch angle is an important parameter, so operating the wind turbines at a high pitch angle may reduce the risk of icing

but will cause a drop in power output, so a compromise must be reached. Xie et al.¹⁸ studied in their article the attachment of ice to the surface of two profiles (symmetrical and antisymmetric) under different icing situations. It has been found that ice fixations on the leading edge have the greatest effect on aerodynamic performance than other locations. They also indicated that the aerodynamic performance of the attachment is more important whenever icing time is long. In their study two types of

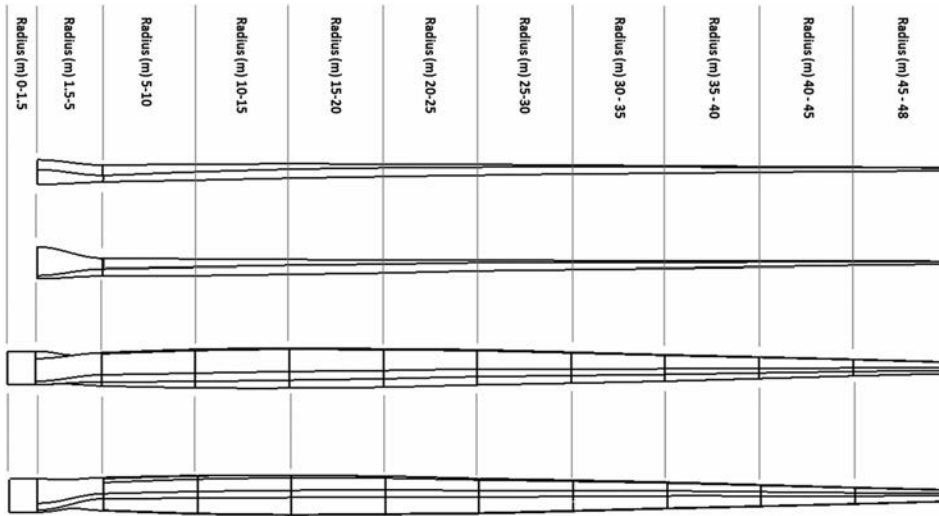


FIGURE 6 Partitions of the blade in terms of radius from the root

ice were taken into account, the symmetrical aerodynamic profile (NACA 0012), which is more easily modified by the attachment of glaze, while the asymmetrical profile (NACA 4412) in his turn is affected by the attachment of rime. Wang¹⁹ has evaluated experimentally the formation of ice in a large refrigerated wind tunnel on a three-bladed turbine model, where different parameters have been measured via a data acquisition system and recorded by Labview software. Several pitch angles have been tested in their article where 11.42° represents the optimal angle that was used in different icing conditions for two types of ice (glaze and rime). Sixty two percentage of power loss was reported for 94 mm thickness of glaze type, while 20% loss was indicated for 8.5 mm rime. Alsabagh²⁰ presented in his thesis the impact of atmospheric ice accumulation on the aerodynamic performance of wind turbine blades. The rotor of a three-bladed turbine was digitally simulated using ANSYS software. The material used is an ultra-light carbon-reinforced fiber. Three different icing scenarios were identified to study the vibration behavior of the wind turbine blade and rotor. At the leading edge of the blade, ice loads were applied and the natural frequencies of clean and iced blades were compared. To see the influence of ice accretion on the fatigue life of the blade structure, the severe icing scenario R8 was selected and showed a remarkable reduction in fatigue life due to increased Von Mises stresses and dynamic amplification factor under three icing loads. A computational fluid dynamics (CFD) analysis was conducted for different icing scenarios, an increase in drag and a decrease in the lift were observed, resulting in a considerable reduction in power generation.

Until now, the icing mechanism remains complicated and incomprehensible, so there is a need for more in-depth research in this direction. This work has been

focused on the mechanical behavior of wind turbines blades by examining the changes in structural and aerodynamic properties caused by the formation of ice. The problem of the design of wind turbine blades has been also treated using ABAQUS software based on the finite element method taking into account aerodynamic, centrifugal and inertial loads under the conditions of service of the blade. The stiffness and strength of the blade under different loading modes has been studied using Carbon (CC) fibers, Glass (GG) fibers and hybrid Carbon-Glass (CG). The results of this study may subsequently assist in the development of icing prevention techniques.

2 | CONCEPTION OF WIND TURBINE

2.1 | Design and construction

The Horizontal Axis Wind Turbine (HAWT) used in this research work has a predicted rated power of 5 MW with a blade diameter of 48 m. The general specifications of the studied blade model are presented in Table 1. In commerce, a study of examples available allowed us to obtain the aerodynamic characteristics, where we have at our disposal a lot of information such as chord distribution curves, torsion, pre-bend, thickness, and distance between the pitch axis and the trailing edge of various blades utilized. Based on these data, we averaged them to obtain the values used to develop the numerical model and then define the blade profiles. The standard DU airfoils was selected and was developed by the Delft University of Technology in the Netherlands.²¹ Figure 2 illustrates the distribution of the profiles in the wind turbine blade. The circular part is connected to the hub and then the transition portion; the other sections use the

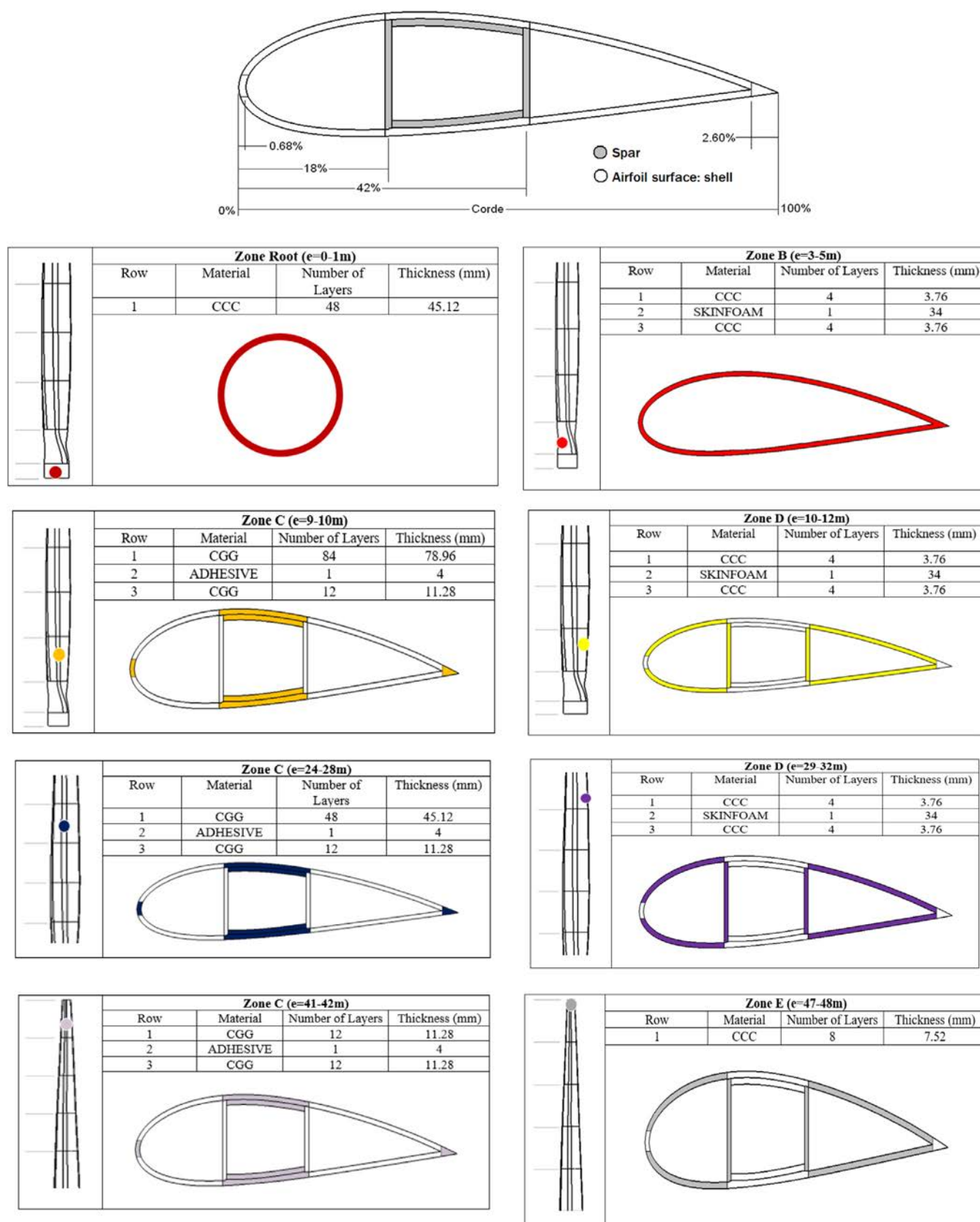


FIGURE 7 Example of the distribution of materials in the section of the wind turbine blade [Colour figure can be viewed at wileyonlinelibrary.com]

DU-00-W2-401, DU-91-W2-250, DU-93-W-210 profiles for the blade design of horizontal axis wind turbines.²² These airfoils were chosen for its high lift to drag ratio and its consistency at various Reynolds number, Figure 3.

The fabrication of wind turbine blades is mainly characterized by a technique of assembly and bonding between the lower and the upper surface (Intrados/Extrados), which are joined by two shear webs.²³ In what follows, the blade has been divided into different zones as shown in Figure 4 to create partitions allowing multiple combinations (thickness and orientation of successive layers) of the materials used according to the need.²⁴

TABLE 3 Mechanical properties of Skinfoam and Adhesive³³

	Skinfoam	Adhesive
ρ (kg/m ³)	200	1200
E (MPa)	256	3000
ν	0.3	0.3

2.2 | Methods of fabrication

Recently, Siemens has implemented a one shot manufacturing process employing an inflatable male mould to eliminate the gluing of intrados to the extrados.²⁵ To increase the stiffness of the blades, hybrid designs of composite steel blades were developed by Enercon. The designers utilize the directional properties of the composites in order to develop bend-torsion coupled designs, to induce twist while the blade bends when it is exposed to wind loads. This is done in order to automatically adjust the pitch of the blade when the wind changes abruptly and short enough to not give the pitch control mechanism sufficient time to respond.²⁶ Other designs are oriented towards pre-bent blades which straighten out under operational wind loads.²⁷ There are also blades made with hybrid fiber mats. An example shows a blade fabricated with a carbon-glass hybrid tri-axial mat with the given fiber alignments such as $[-45^\circ_{\text{Glass}}/0^\circ_{\text{Carbon}}/+45^\circ_{\text{Glass}}]$,²⁸ helps to maintain the carbon fibers straight and thus contributes to the buckling resistance of the blade. Figure 5 illustrates the

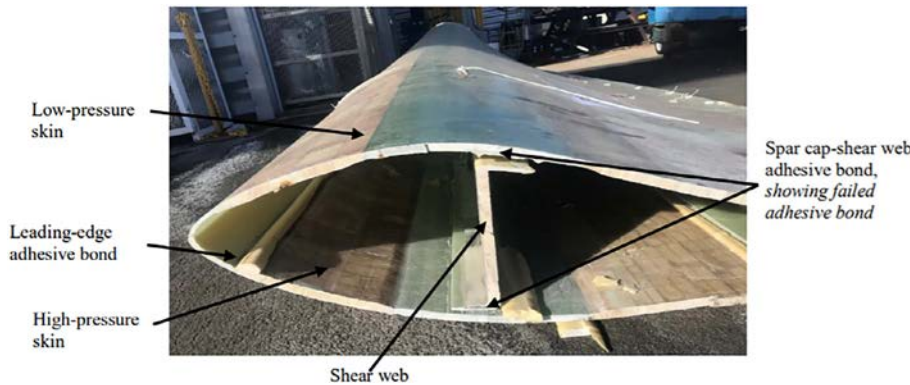


FIGURE 8 Bonding process of composite wind turbine blades³⁴
[Colour figure can be viewed at wileyonlinelibrary.com]

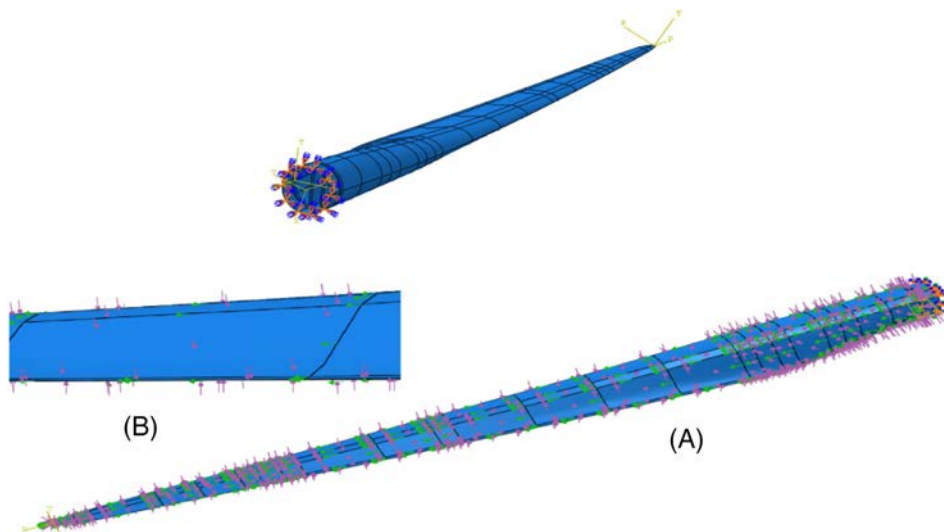


FIGURE 9 Encastre boundary condition and loads applied on the wind turbine blade
[Colour figure can be viewed at wileyonlinelibrary.com]

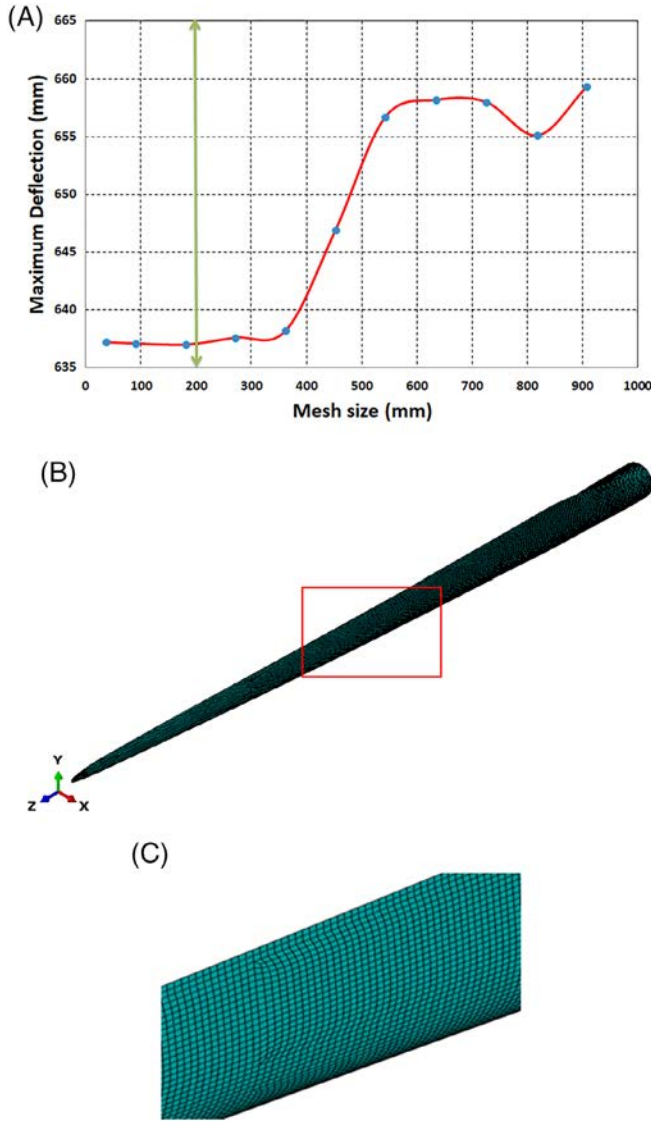


FIGURE 10 A, Convergence curve for the blade mesh according to its deflection at the free end, B, Mesh convergence, C, Zoom of the Mesh [Colour figure can be viewed at wileyonlinelibrary.com]

different steps (phases) during the fabrication of a composite blade.

2.3 | Materials

Composite materials are gradually being employed in specific applications because of their excellent “mass/rigidity” relationships compared to traditional materials.^{29,30}

The most common wind turbine blades are constructed from Glass fibers reinforced with polyester or epoxy resin. In recent years, Carbon fibers attracted a

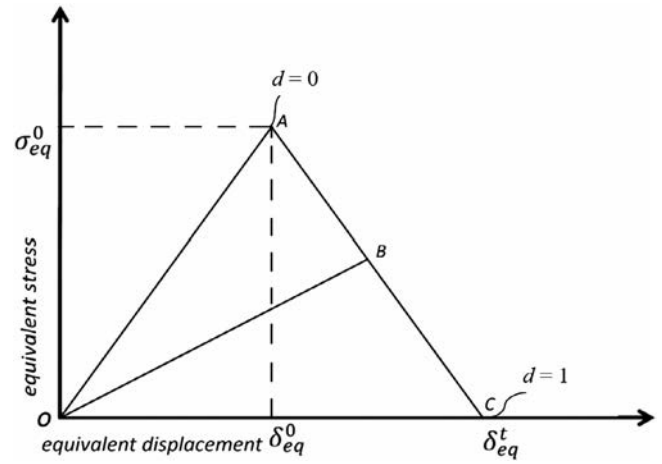


FIGURE 11 Damage evolution law⁴²

growing interest due to their low price and the important requirements presented by the larger rotor blades.³¹

To make a comparison and in order to know which of them satisfies our industrial expectations and requirements, two composite materials were used. Their properties are shown in Table 2.^{29,32}

The materials adopted for the conception of the blade structure are a combination of sandwiches and laminates whose orientation $[0^\circ/-45^\circ/45^\circ/0^\circ]$ is applied to the current model. Figures 6 and 7 represent, respectively, the distribution of the 48 m long wind turbine blade adopted in this work and some examples of the distribution of materials in each section.

The composite lamination of the blade is also composed of foam core material (SKINFOAM) whose mechanical properties are indicated in Table 3.³³

Taking into account the gluing between the shear webs and the blade, Figure 8. An isotropic material is added to the structure, its properties are reported in Table 3.³³

2.4 | Boundary conditions

Finite element models of wind turbine blades must eventually integrate all structural properties and boundary conditions applied closely to real cases. Figure 9 illustrates the boundary condition assigned to the blade using “Encastre” type applied at the root to reduce the computational requirements.³⁵ The blade is fixed at one end to act as a cantilever while the other end is free. Figure 9A shows also a blade under all loads, where the green arrows are for centrifugal load and the purple ones for the aerodynamic load. Figure 9B is an enlargement of a section of the blade.

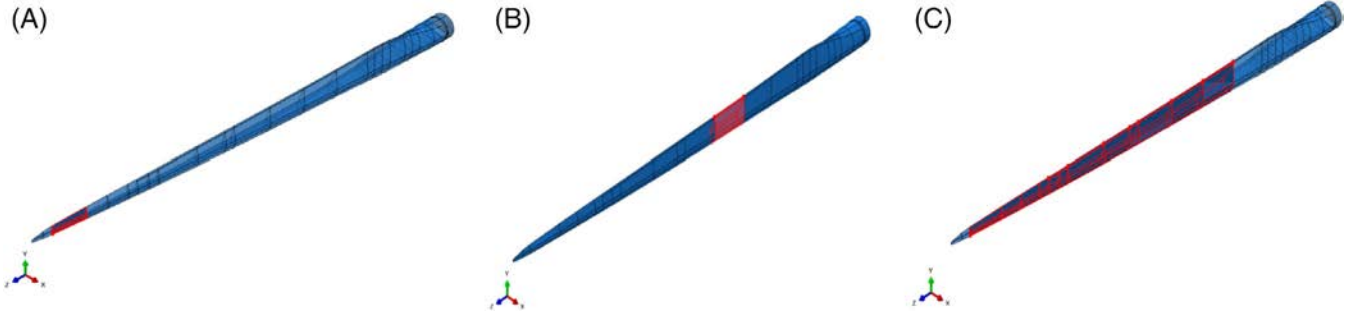


FIGURE 12 Ice layer deposition scenarios on the blade [Colour figure can be viewed at wileyonlinelibrary.com]

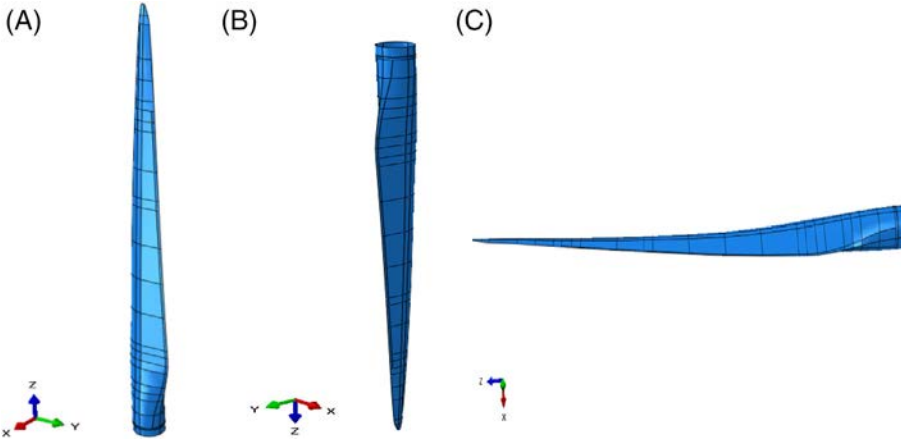


FIGURE 13 Blade position [Colour figure can be viewed at wileyonlinelibrary.com]

3 | NUMERICAL MODEL

3.1 | Mesh convergence

For the model designed, shell elements type (S4R) was adopted. Based on the study on the maximum deflection at the blade tip, the convergence of the mesh will be investigated. Uniform pressure distribution of 1 kPa is applied to the blade while its root is fixed. The plot in Figure 10 represents the variation of the deflection at the free end against the mesh size indicates a mesh size of 200 mm and finer the size begins to converge. This mesh size corresponds to a “mesh size/structure size” ratio of “ l_e/l_s ,” which is 0.005. This value or smaller will be retained for more detailed researches in order to avoid mesh convergence studies for each case.³⁶

3.2 | Failure mode of the composite material

The intra-ply damage mechanisms in this work are derived from Hashin failure criteria which mostly occurs in two different phases: damage initiation and damage evolution law.³⁷

3.2.1 | Damage initiation

Hashin's theory distinguishes between fiber and matrix failure, based on four possible modes in which the material might fail: tensile fiber failure (HSNFTCRT), compressive fiber failure (HSNFCCRT), tensile matrix failure (HSNMTCRT), and compressive matrix failure (HSNMCRT).

The initiation criteria are defined as follows^{38,39}:

- Mode 1: Tensile fiber failure for $\sigma_{11} \geq 0, f_1 \geq 1$

$$\left(\frac{\hat{\sigma}_{11}}{X_T}\right)^2 + \alpha \times \left(\frac{\hat{\sigma}_{12}}{S_{LT}}\right)^2 = f_1 \quad (1)$$

- Mode 2: Compressive fiber failure for $\sigma_{11} < 0, f_2 \geq 1$

$$\left(\frac{\hat{\sigma}_{11}}{X_c}\right)^2 = f_2 \quad (2)$$

- Mode 3: Tensile matrix failure for $\sigma_{22} + \sigma_{33} > 0, f_3 \geq 1$

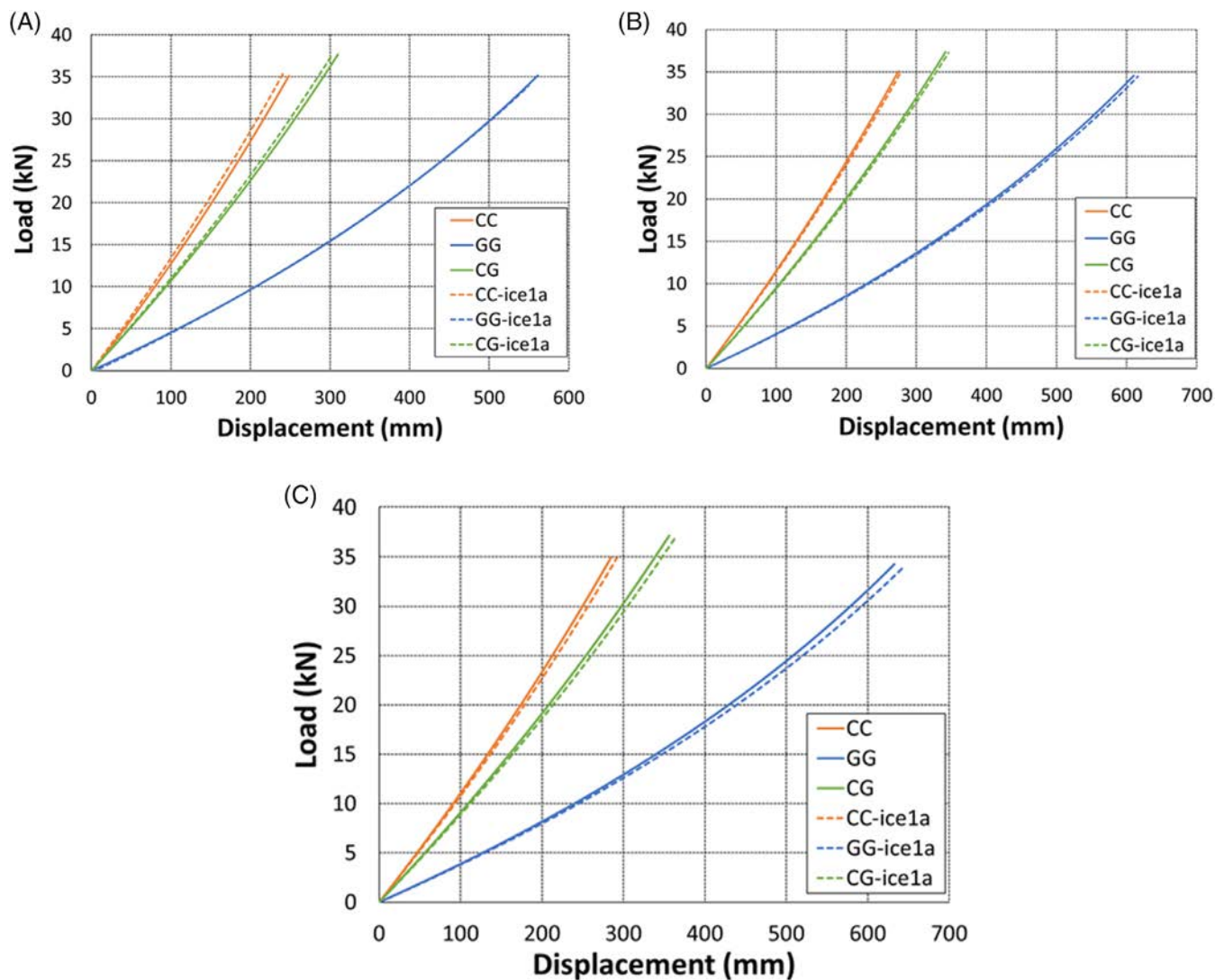
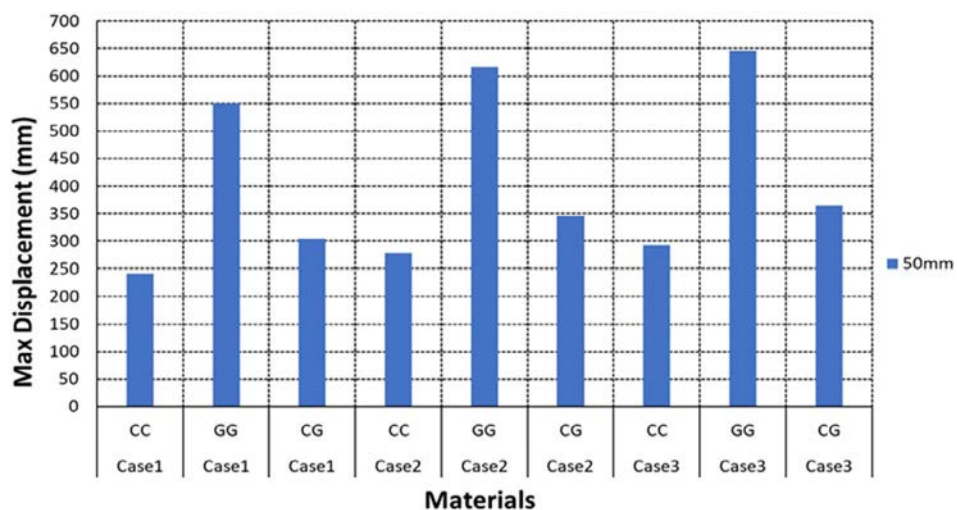


FIGURE 14 Mechanical behavior of the blade with and without ice for a thickness of 50 mm, Ice-1a [Colour figure can be viewed at wileyonlinelibrary.com]

FIGURE 15 Comparison of the maximum displacement of the iced blade according to different composite materials, ($a = 50$ mm) [Colour figure can be viewed at wileyonlinelibrary.com]



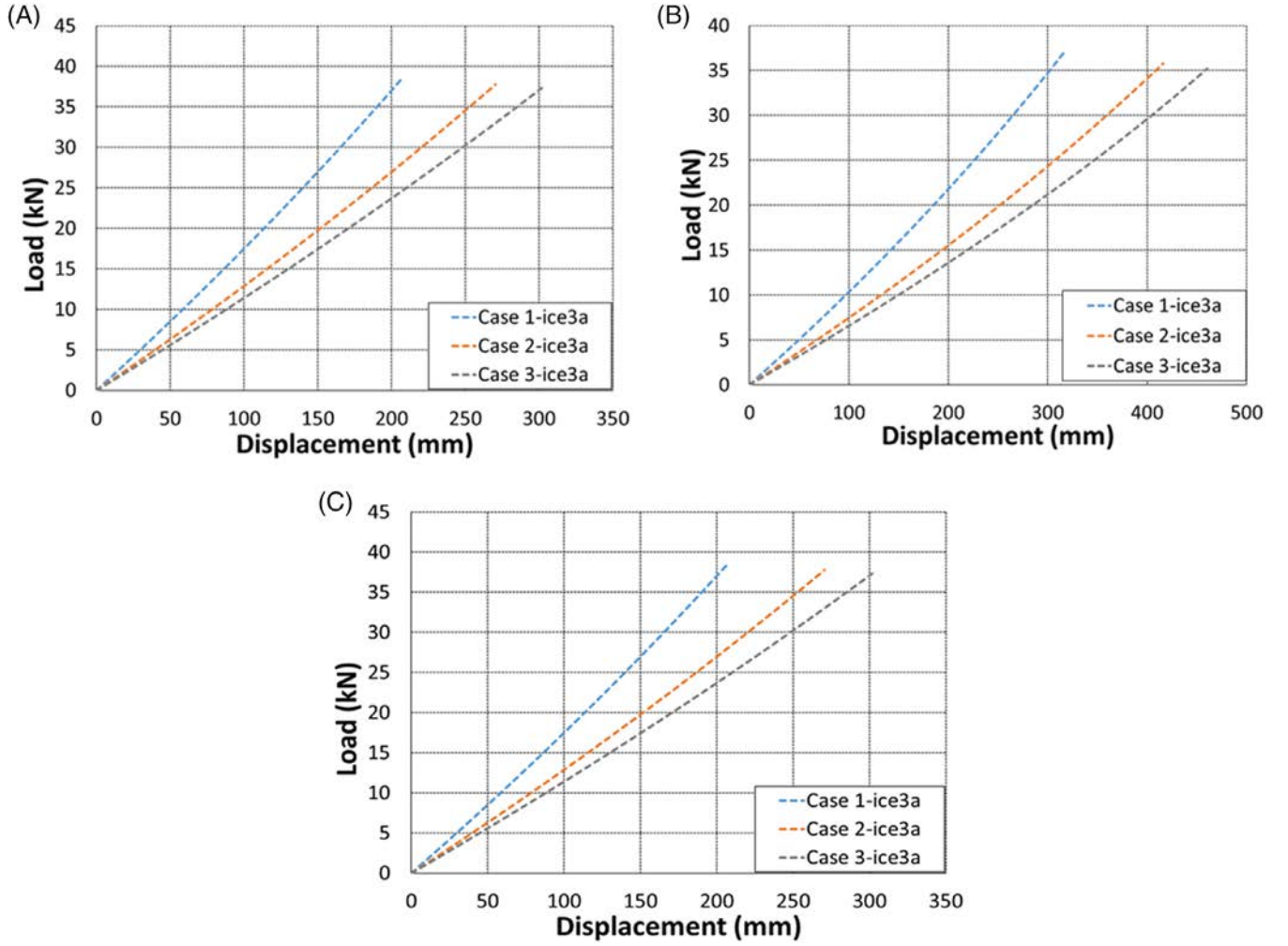


FIGURE 16 Behavior of the iced blade with a 50 mm layer of ice for different materials, Ice-3a [Colour figure can be viewed at wileyonlinelibrary.com]

TABLE 4 Maximum displacement of the 3 cases of the composite blade, with a 50 mm layer of ice

	Max Displacement (mm)		
	CC	GG	CG
Case 1	161.025	316.963	206.951
Case 2	218.054	415.944	270.335
Case 3	244.509	460.561	301.876

$$\left(\frac{\hat{\sigma}_{22}}{Y_T}\right)^2 + \left(\frac{\hat{\sigma}_{12}}{Y_T}\right)^2 = f_3 \quad (3)$$

- Mode 4: Compressive matrix failure for $\sigma_{22} + \sigma_{33} < 0, f_4 \geq 1$

$$\left(\frac{\hat{\sigma}_{22}}{2S_{TT}}\right)^2 + \left[\left(\frac{Y_c}{2S_{TT}}\right)^2 - 1\right] \times \frac{\hat{\sigma}_{22}}{Y_c} + \left(\frac{\hat{\sigma}_{12}}{S_{LT}}\right)^2 = f_4 \quad (4)$$

Where:

X_T, X_c are respectively the tensile and compressive strengths in the fibers direction, Y_T, Y_c are the tensile and compressive strengths in the transverse direction.

S_{LT}, S_{TT} indicates the longitudinal and the transverse shear strengths of the composite.

$\hat{\sigma}_{11}, \hat{\sigma}_{22}, \hat{\sigma}_{12}$ determines the contribution of shear stress on the stress tensor and α is the contribution of shear stress to the initiation of fiber tensile failure mode.⁴⁰

3.2.2 | Damage evolution

Damage evolution is used, which makes it possible to describe the behavior of the materials after the start of

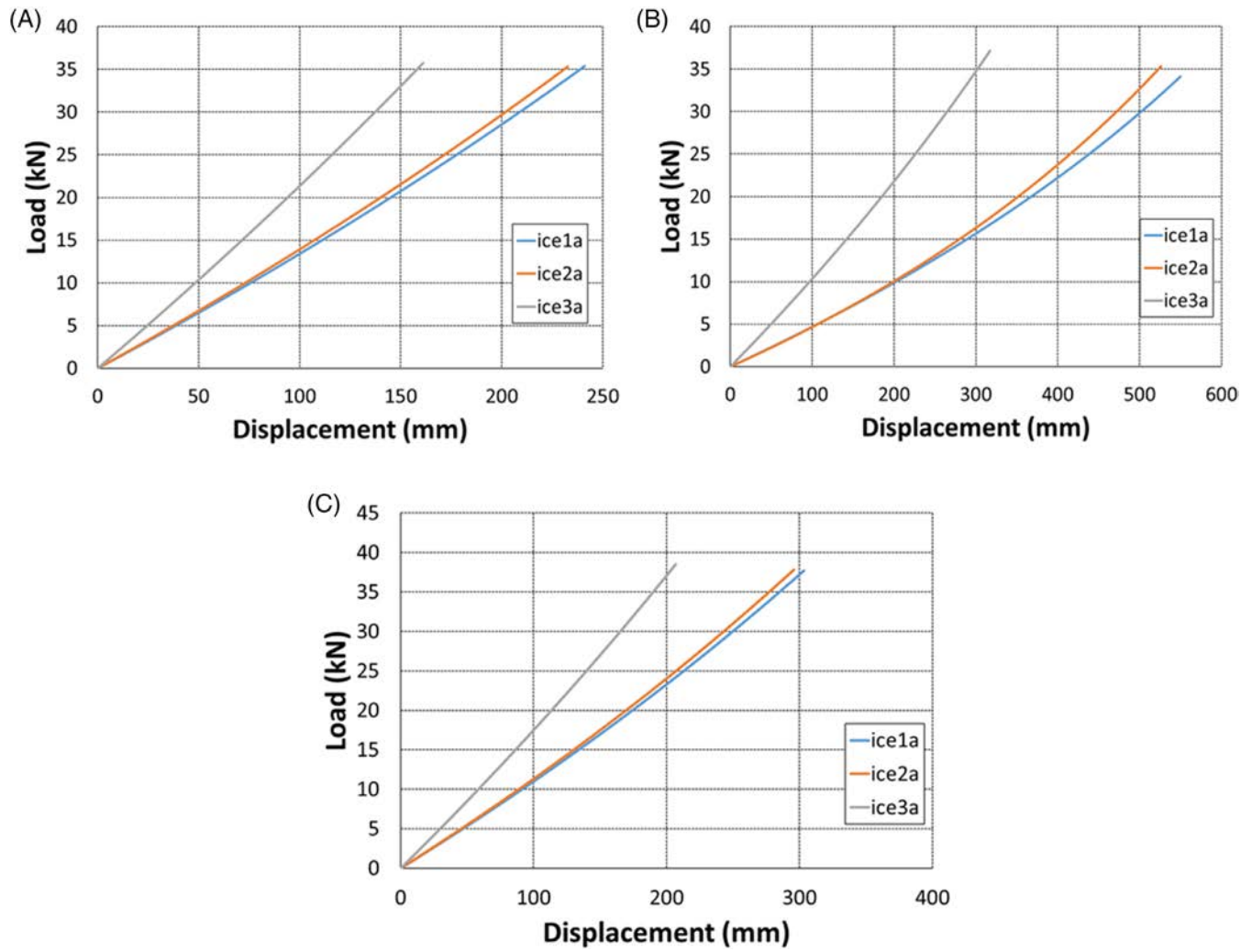


FIGURE 17 Effect of the ice layer thickness for different materials, Case 1 [Colour figure can be viewed at wileyonlinelibrary.com]

TABLE 7 Damage values given by the Hashin criterion, CG blade with ice

		HSNFCRT	HSNFTCRT	HSNMCCRT	HSNMTCRT
Case 1	Ice-1a	1.67×10^{-3}	7.71×10^{-3}	2.33×10^{-2}	1.09×10^{-1}
	Ice-2a	1.66×10^{-3}	7.65×10^{-3}	2.31×10^{-2}	1.08×10^{-1}
	Ice-3a	1.61×10^{-3}	7.46×10^{-3}	2.19×10^{-2}	9.97×10^{-2}
Case 2	Ice-1a	1.82×10^{-3}	8.45×10^{-3}	2.68×10^{-2}	1.40×10^{-1}
	Ice-2a	1.84×10^{-3}	8.54×10^{-3}	2.71×10^{-2}	1.41×10^{-1}
	Ice-3a	1.89×10^{-3}	8.83×10^{-3}	2.86×10^{-2}	1.53×10^{-1}
Case 3	Ice-1a	4.77×10^{-3}	2.32×10^{-2}	7.66×10^{-2}	2.35×10^{-1}
	Ice-2a	5.05×10^{-3}	2.45×10^{-2}	8.11×10^{-2}	2.44×10^{-1}
	Ice-3a	1.26×10^{-2}	4.69×10^{-2}	1.57×10^{-1}	3.75×10^{-1}

the damage and to calculate the stiffness of the damaged elements, Figure 11.³⁵

The evolution of each damage variable is conditioned by an equivalent displacement. We presume that for each

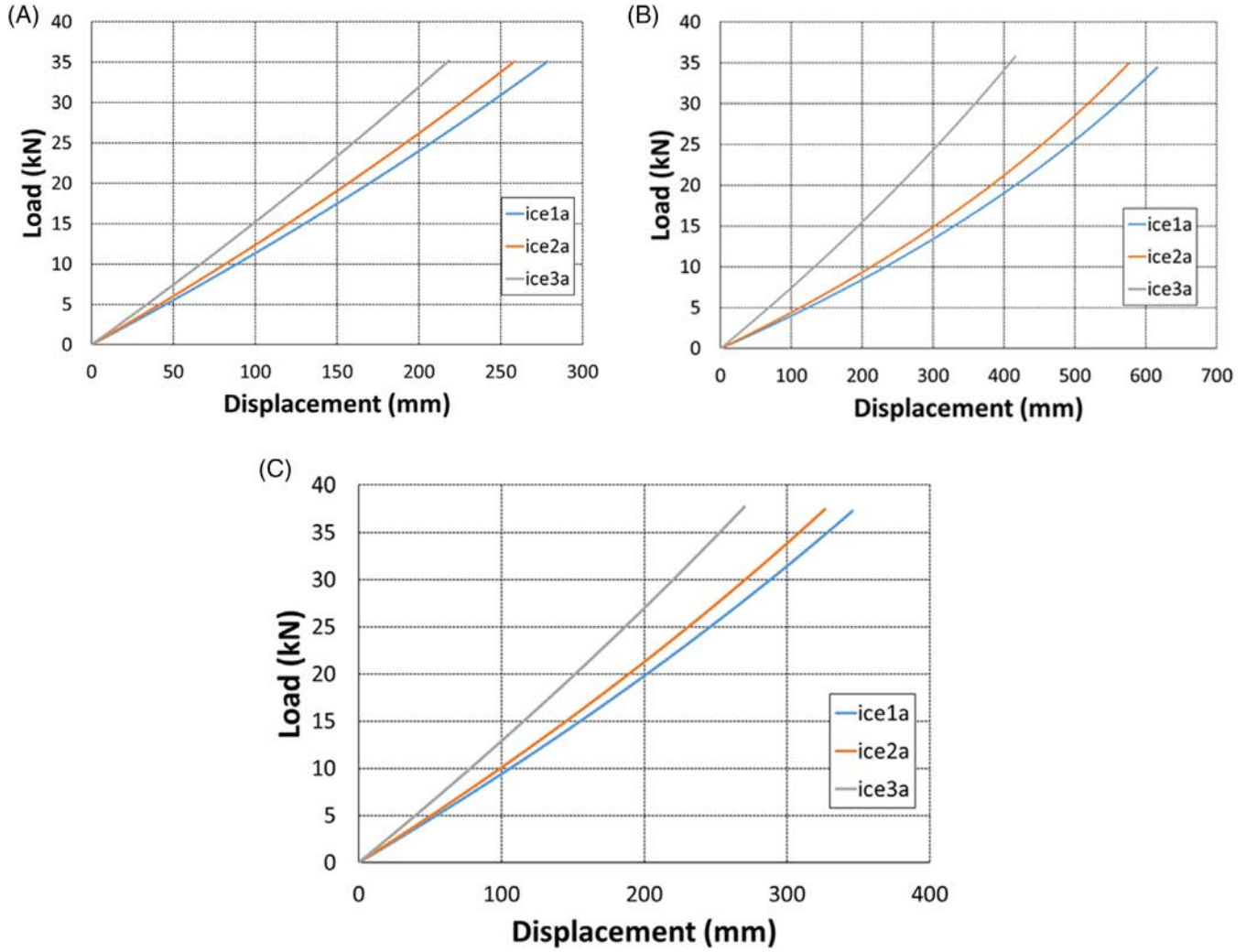


FIGURE 18 Effect of the ice layer thickness for different materials, Case 2 [Colour figure can be viewed at wileyonlinelibrary.com]

failure mode, the damage variable is specified by the equation below⁴¹:

$$d = \frac{\delta_{eq}^f (\delta_{eq} - \delta_{eq}^0)}{\delta_{eq} (\delta_{eq}^f - \delta_{eq}^0)} \quad (5)$$

In this relation δ_{eq}^0 is the equivalent displacement at which the initiation criterion is achieved, and δ_{eq}^f is the equivalent displacement at which the material is entirely damaged ($d = 1$).⁴⁰

3.3 | Critical loading

The rotor blades are exposed to different loads that act on their structures. The types of loads to which a wind

turbine is subjected during its operation can be defined as follows^{43,44}:

- Aerodynamic load originating from the force of the wind.
- Inertial load due to blade weight.
- Centrifugal loads resulting from the rotation of the rotor system.

However, for the rest of this work, the model studied is a 48 m long industrial WTB modelled using conventional shell elements. In order to get closer to the real case, 3 loads were applied at the same time using the ABAQUS software. The objective is to analyze the behavior of the blade using each time Carbon (CC) fibers and Glass fibers (GG), and also to see the effect of the hybrid Carbon-Glass (CG) localized at section C of a Carbon blade as shown previously in Figure 4.

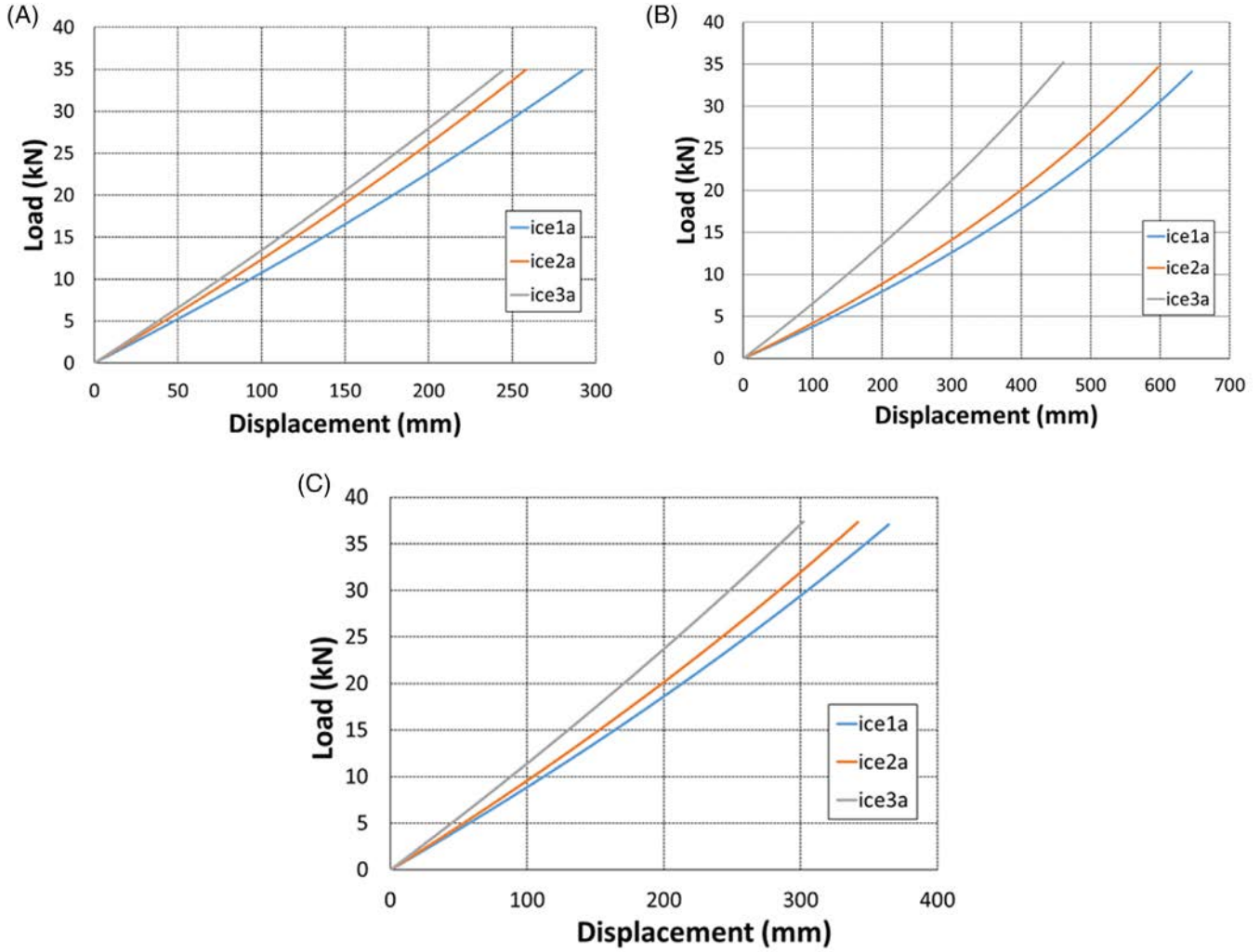


FIGURE 19 Effect of the ice layer thickness for different materials, Case 3 [Colour figure can be viewed at wileyonlinelibrary.com]

Ice is analysed at three different locations:

- Configuration 1: Ice is on the blade tip side (length of ice layer: 3.213 m, distance from rotor: 43.031 m), Figure 12A.
- Configuration 2: Ice is on the central part of the blade (length of ice cover: 4.014 m, distance from rotor: 20.003 m), Figure 12B.
- Configuration 3: Ice is over a large part of the blade (length of ice cover: 30.318 m, distance from rotor: 16.017 m), Figure 12C.

3.3.1 | Aerodynamic loading

The aerodynamic load is engendered by the lift and drag of the blade airfoil, which is calculated using (BEM) theory for each blade element. Using the ABAQUS software,

the forces are thus calculated and applied homogeneously along the section of the blade.⁴⁵

3.3.2 | Centrifugal loading

The centrifugal force applied to the blade is caused by the rotation of the rotor at an angular velocity (ω). This force is calculated using the Equation (6).^{43,45}

$$F_c = \frac{1}{2} m \times \omega^2 r \quad (6)$$

where ω , m , r are, respectively, the rotational velocity, the mass of the blade and the distance of the blade element from the center of rotation.

Equation (7) is used to find the centrifugal force for each element along the length of the blade and the stress caused.

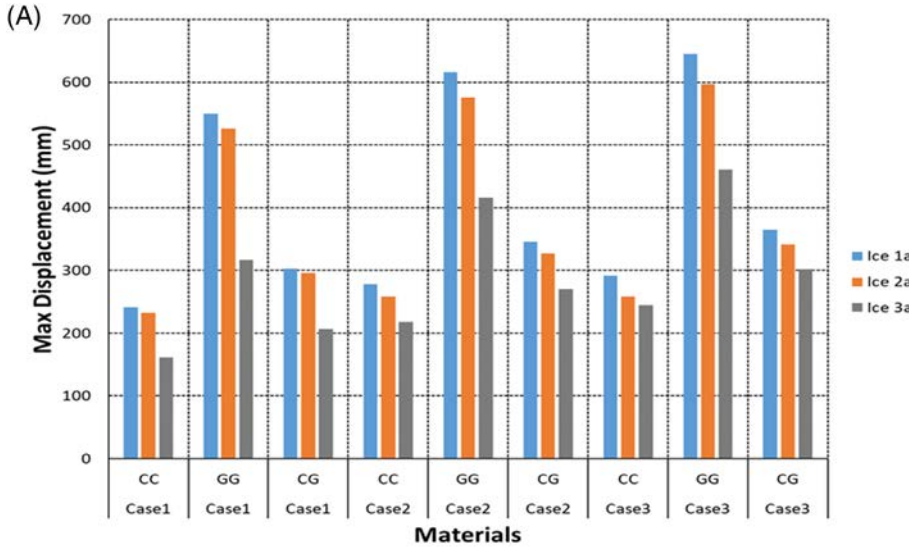
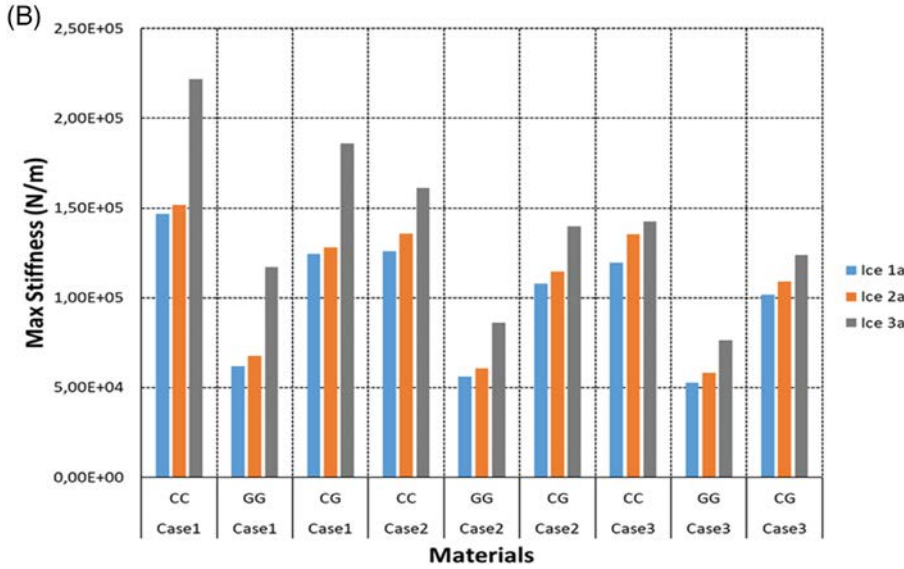


FIGURE 20 A, Maximum displacement, B, Maximum stiffness of the 3 cases of the composite blade for different configurations of ice [Colour figure can be viewed at wileyonlinelibrary.com]



$$F_c = \frac{\omega^2}{2} \int m_s r dr \quad (7)$$

m_s is the mass of the section.

3.3.3 | Inertial loading

Gravity loads are the main loads affecting the wind turbine blade during operation and can exert high fatigue stresses on the moving rotor. After defining the materials, ABAQUS software will determine the load in function of the layups parameters. Equation 8 gives the mass of the structure.^{36,46}

$$\text{Mass} = \sum \text{Volume of material}_i \times \text{Density of material}_i \quad (8)$$

Once the blade is loaded by the various forces mentioned above, three-blade positions are simulated:

- *Case* Blade in a vertical position pointing upwards, Figure 13A.
- *Case* Blade in a vertical position pointing downwards, Figure 13B.
- *Case* Blade in a horizontal position, Figure 13c.

4 | SIMULATION RESULTS AND DISCUSSIONS

4.1 | Material effect

Once the loads were determined and quantified, the effect of ice on the wind turbine blades has been studied and several numerical tests evaluated the behavior of different composite materials. First, configuration 1 was selected with an ice thickness of 50 mm (Ice-1a).

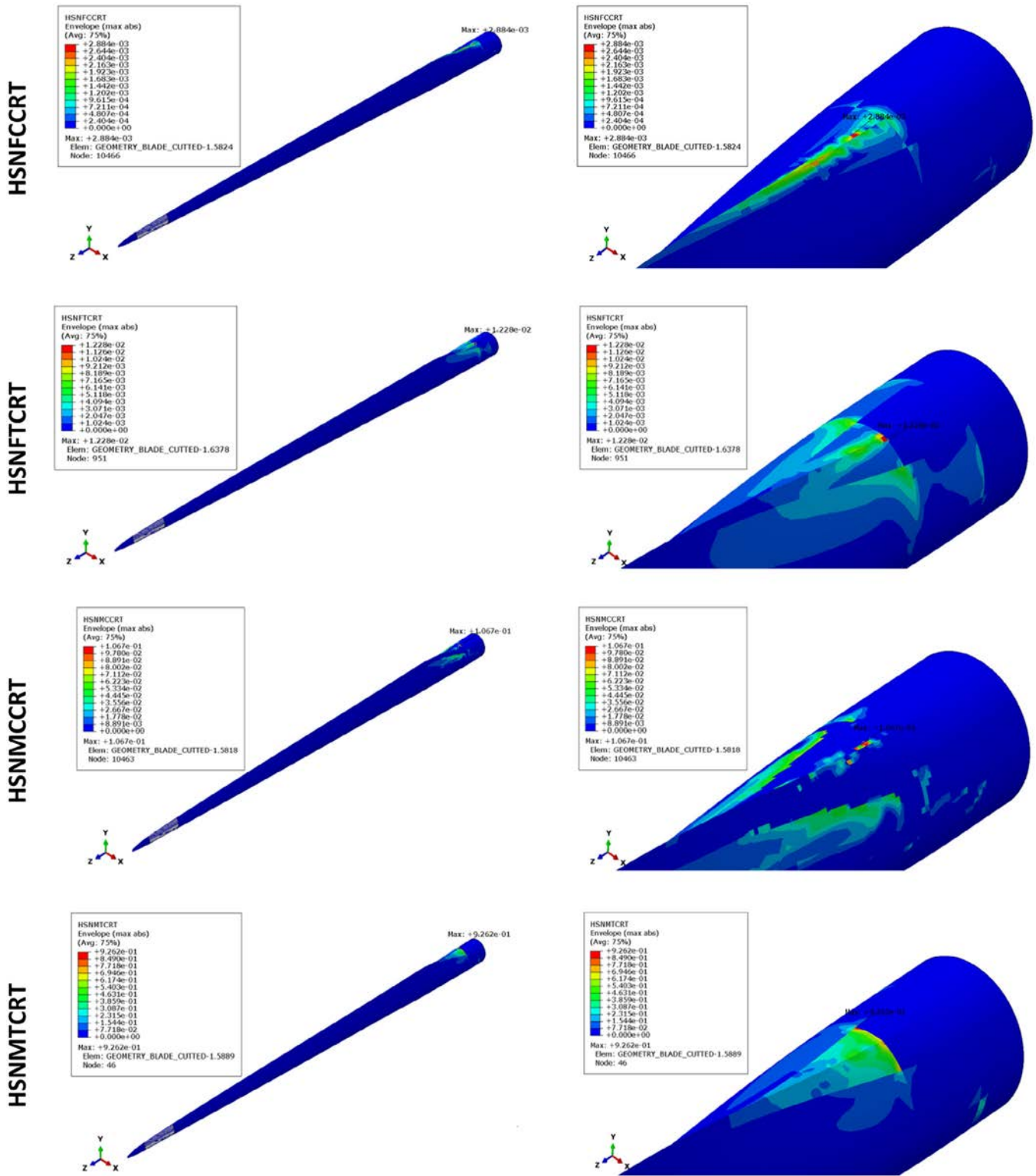


FIGURE 21 Hashin's Criterion, GG Blade with ice (Ice-1a), Case 1 [Colour figure can be viewed at wileyonlinelibrary.com]

From Figure 14, the load-displacement curves show that the CC is the most resistant to the mechanical loads exerted on the blade during operation. This material moves the least in comparison to GG and CG and has a maximum force value at about 35.36

kN for the iced blade and 35.33 kN for the clean in case 1. It can also be seen that the formation of a 50-mm thick layer of ice at the blade tip has a negligible effect on the structure when it is suspended vertically.

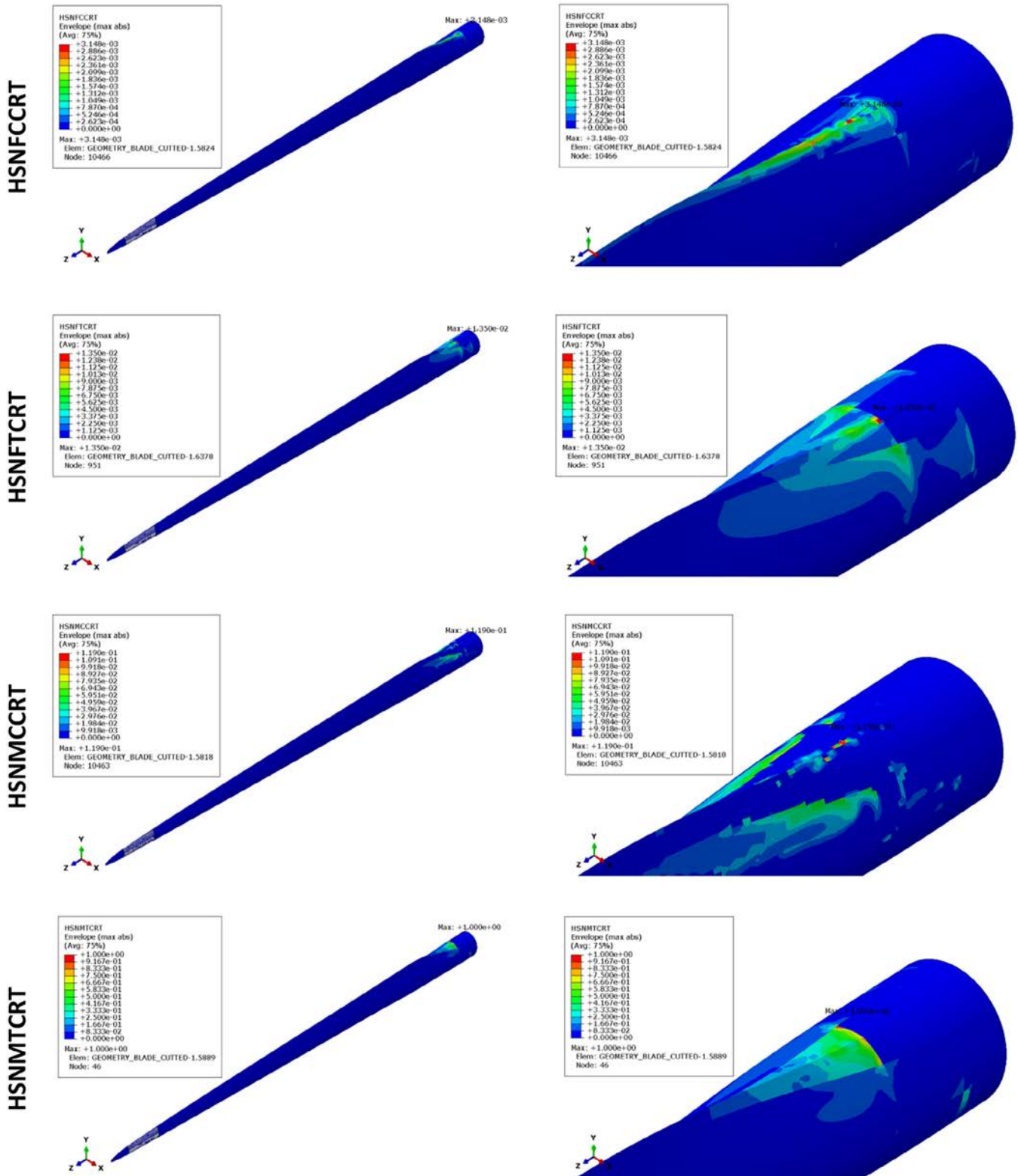


FIGURE 22 Hashin's Criterion, GG Blade with ice (Ice-1a), Case 2 [Colour figure can be viewed at wileyonlinelibrary.com]

In order to better visualize the results, a histogram has been presented in Figure 15 to compare the maximum displacement of the blade for different composite materials considering that the ice has a thickness of 50 mm at the tip of the blade. It was observed clearly

that the highest value (645.492 mm) is given by the GG material when the iced blade is horizontal, while the lowest displacement (240.961 mm) was detected for a CC blade positioned vertically pointing upwards, case 1.

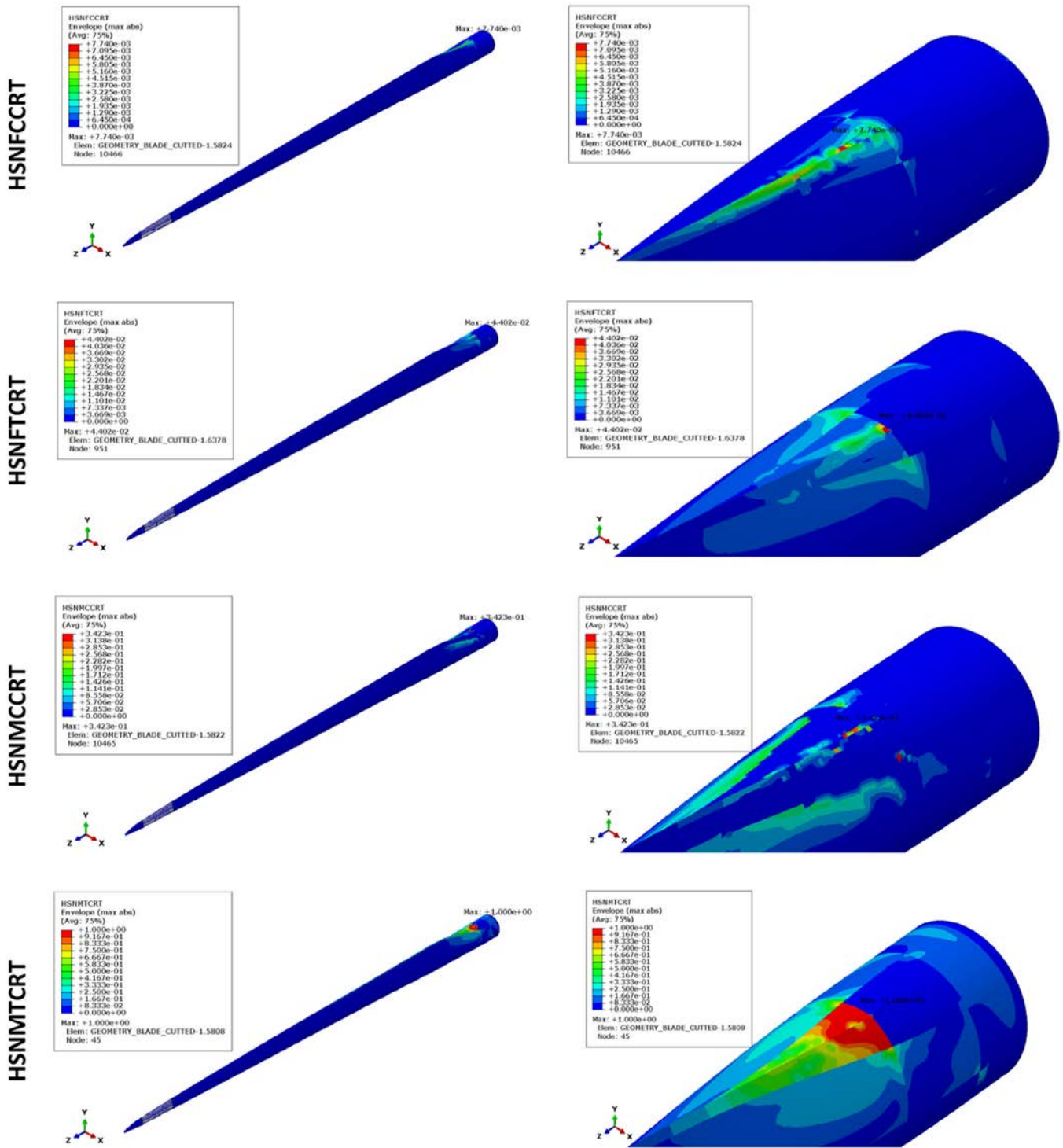


FIGURE 23 Hashin's Criterion, GG Blade with ice (Ice-1a), Case 3 [Colour figure can be viewed at wileyonlinelibrary.com]

4.2 | Blade position effect

In order to visualize the effect of the blade position, this time we opted for the third configuration with an ice thickness of 50 mm (Ice-3a).

Based on Figure 16 and Table 4, it was noted that despite the material changes when the structure is placed vertically with the tip upwards (case 1) its displacement decreases. The smallest and largest maximum displacements are respectively 161.025 mm for a vertical Carbon

TABLE 5 Damage values given by the Hashin criterion, CC blade with ice

		HSNFCCRT	HSNFTCRT	HSNMCCRT	HSNMTCRT
Case 1	Ice-1a	1.51×10^{-3}	7.07×10^{-3}	2.11×10^{-2}	5.03×10^{-2}
	Ice-2a	1.49×10^{-3}	6.97×10^{-3}	2.08×10^{-2}	4.95×10^{-2}
	Ice-3a	1.44×10^{-3}	6.76×10^{-3}	1.97×10^{-2}	4.81×10^{-2}
Case 2	Ice-1a	1.64×10^{-3}	7.77×10^{-3}	2.40×10^{-2}	5.52×10^{-2}
	Ice-2a	1.65×10^{-3}	7.80×10^{-3}	2.41×10^{-2}	5.55×10^{-2}
	Ice-3a	1.71×10^{-3}	8.08×10^{-3}	2.55×10^{-2}	5.74×10^{-2}
Case 3	Ice-1a	3.98×10^{-3}	1.98×10^{-2}	6.25×10^{-2}	1.40×10^{-1}
	Ice-2a	4.19×10^{-3}	2.07×10^{-2}	6.57×10^{-2}	1.47×10^{-1}
	Ice-3a	9.23×10^{-3}	4.09×10^{-2}	1.30×10^{-1}	2.89×10^{-1}

TABLE 6 Damage values given by the Hashin criterion, GG blade with ice

		HSNFCCRT	HSNFTCRT	HSNMCCRT	HSNMTCRT
Case 1	Ice-1a	2.88×10^{-3}	1.23×10^{-2}	1.07×10^{-1}	9.26×10^{-1}
	Ice-2a	2.87×10^{-3}	1.22×10^{-2}	1.06×10^{-1}	9.24×10^{-1}
	Ice-3a	2.82×10^{-3}	1.21×10^{-2}	1.04×10^{-1}	8.99×10^{-1}
Case 2	Ice-1a	3.15×10^{-3}	1.35×10^{-2}	1.19×10^{-1}	1.00×10
	Ice-2a	3.18×10^{-3}	1.37×10^{-2}	1.21×10^{-1}	1.00×10
	Ice-3a	3.29×10^{-3}	1.42×10^{-2}	1.26×10^{-1}	1.00×10
Case 3	Ice-1a	7.74×10^{-3}	4.40×10^{-2}	4.40×10^{-1}	1.00×10
	Ice-2a	8.32×10^{-3}	4.81×10^{-2}	3.70×10^{-1}	1.00×10
	Ice-3a	2.82×10^{-2}	1.28×10^{-1}	7.05×10^{-1}	1.00×10

(CC) blade (case 1) and 460.561 mm for a horizontal Glass (GG) blade (case 3).

4.3 | Effect of the position of the ice layer

In order to determine the optimal blade position during the ice accretion phenomenon, one chooses to change the blade position (case 1, case 2 and case 3) for the 3 ice configurations (Ice-1, Ice-2 and Ice-3) for the same thickness of ice which is equal to 50 mm.

It is obvious to signal that the position and mass of the ice in severe icing conditions are interesting parameters that can lead to blade failure.

From Figures 17, 18 and 19, it is clear that configuration 3 is more influenced by the formation of ice because it covers a large part of the blade and is homogeneously distributed, which allows it to always have the smallest maximum displacement value despite the change in material.

The CC blade containing 50 mm of ice (Ice-3a) showed the lowest maximum displacement value

(161.025 mm) compared to GG and CG, Figure 20A. It is the one that resists the most to the deformation in response to the applied forces. Carbon (CC) fibers have detected the highest maximum stiffness value which is equal to 3.217×10^5 N/m for the configuration 3 when the iced blade is vertical, pointing upwards Figure 20B.

Based on the damage model used for the different composite materials, as shown in Tables 5, 6, and 7, we notice that the Glass (GG) blade reaches full damage at a unit value in matrix tension mode (HSNMTCRT) in both cases 2 and 3, which implies the initiation of damage.

Figures 21, 22, and 23 show the damage that occurred respectively in the GG blade where the critical location for all failure criteria is represented by the red color. It is clear that at the blade root the stresses are concentrated due to the thickness transitions near the area where the blades are joined to the hub.

The damage of the spars is attributed to the low resistivity of the adhesive present during the blade manufacturing process when joining the two halves (Intrados/Extrados).

Carbon (CC) fibers are the most resistant to the mechanical loads exerted on the blade during operation. This material is the one that moves the least compared to Glass (GG) fibers and hybrid Carbon-Glass (CG). The smallest maximum displacement of 161.025 mm was detected for a vertical Carbon (CC) blade pointing upwards. It was also found that the formation of a 50-mm thick layer of ice at the end of the blade has a negligible effect on the structure when suspended vertically. It is also noted that configuration 3 is more influenced by the formation of ice, as it envelops a large part of the blade and is evenly and homogeneously distributed, which allows it to always have the smallest maximum displacement value despite the change in material. It was found that the Glass (GG) blade reaches full damage at a unit value in matrix tension mode (HSNMTCRT) in both cases 2 and 3 and that the stresses are concentrated at the blade root due to the thickness transitions near the area where the blades are joined to the hub.

5 | CONCLUSIONS

This research work treated the problem of ice accumulation on wind turbines blades of 48 m installed in cold climate sites and examined with ABAQUS software using the finite element simulation. During this study, the blade in service was subjected to three critical loads (aerodynamic, centrifugal and inertial loads). The behavior of Carbon (CC) fibers, Glass (GG) fibers, and hybrid Carbon-Glass (CG) materials have been the focus of much attention in this research. Three configurations of ice and three-blade positions were taken into account. Stress, displacement, and Hashin damage criteria were examined in each phase. It is obvious to signal that the position of the ice in severe icing conditions is an interesting parameter that can lead to blade failure. The study revealed that the Carbon (CC) was the most resistant material to the mechanical loads applied during blade rotation, that the configuration 3 where ice-covered homogeneously a large part of the blade proved to be the best, and that the optimal blade position was when the ice structure was placed vertically. The critical location for all failure criteria was in the blade root where the stresses were concentrated due to the thickness transitions and subsequently had to be reinforced. It is therefore essential to develop a de-icing system to ensure the correct operation of wind turbines in cold climates regions.


CONFLICT OF INTEREST

The authors declare no potential conflict of interest.

DATA AVAILABILITY STATEMENT

Data sharing is not applicable to this article as no new data were created or analyzed in this study.

ORCID

Oumnia Lagdani  <https://orcid.org/0000-0002-5182-9340>

REFERENCE

1. Sundén B, Wu Z. On icing and icing mitigation of wind turbine blades in cold climate. *J Energy Resour Technol.* 2015;137(5): 051203.
2. Tarfaoui M, Khadimallah H, Imad A, Pradillon JY. Design and finite element modal analysis of 48m composite wind turbine blade. *Appl Mech Mater.* 2011;146:170-184.
3. Edmond A. M. Climate Change: The Science of Global Warming and our Energy Future 2009, 206.
4. Salimipour E, Yazdani S. Improvement of aerodynamic performance of an offshore wind turbine blade by moving surface mechanism. *Ocean Eng.* 2020;195:106710.
5. Christine Mayer, 2007. Electrothermal Defrosting System for a Wind Turbine Blade: Simulations in a Refrigerated Wind Tunnel and Impact on the Power Produced, Thesis Presented at The University of Quebec In Rimouski.
6. Pieter Jan Jordaens. Icing tests on components exposed to low temperatures in the OWI-Lab climate chamber, 1st 2016. <https://www.sirris.be/fr/blog/essais-de-givrage-sur-composants-exposes-des-basses-temperatures-dans-la-chambre-climatique-de>
7. Sudhakar G. Detection of Blade Icing and its Influence on Wind Turbine Vibrations. Ph.D thesis, University of Technology Luleå, Sweden 2019.
8. Latthe SS, Sutar RS, Bhosale AK, et al. Recent developments in air-trapped superhydrophobic and liquid-infused slippery surfaces for anti-icing application. *Prog Org Coat.* 2019;137:105373.
9. Pouryoussefi SG, Mirzaei M, Nazemi MM, Fouladi M, Doostmahmoudi A. Experimental study of ice accretion effects on aerodynamic performance of an NACA 23012 airfoil. *Chin J Aeronaut.* 2016;29(3):585-595.
10. Farid H, Farzaneh M, Saeidi A, Erchiqui F. An atmospheric ice empirical failure criterion. *Cold Reg Sci Technol.* 2018;146: 81-86.
11. Farid H, Farzaneh M, Saeidi A, Erchiqui F. A contribution to the study of the compressive behavior of atmospheric ice. *Cold Reg Sci Technol.* 2016;121:60-65.
12. Fini SH, Erchiqui F, Farzaneh M. Investigating the elastic deformation of wood-plastic composites at cold temperature using the bubble inflation technique. *J Thermoplast Compos Mater.* 2013;28(3):431-441.
13. Fini SH, Erchiqui F, Farzaneh M. Study of the elastic behaviour of wood-plastic composites at cold temperatures using artificial neural networks. *Wood Science and Technology.* 2015; 49(4):695-705.
14. Alsabagh ASY, Tiu W, Xu Y, Virk MS. A review of the effects of ice accretion on the structural behavior of wind turbines. *Wind Engineering.* 2013;37(1):59-70.
15. Pedersen MC, Sørensen H. Towards a CFD Model for Prediction of Wind Turbine Power Losses due to Icing in Cold

- Climate. *Conference: International Symposium on Transport Phenomena and Dynamics of Rotating Machinery, Honolulu, Hawaii, USA*. 2016.
16. Gantasala S, Tabatabaei N, Cervantes M, Aidanpää JO. Numerical investigation of the aeroelastic behavior of a wind turbine with iced blades. *Energies*. 2019;12(12):2422.
 17. Hu L, Zhu X, Hu C, Chen J, Du Z. Wind turbines ice distribution and load response under icing conditions. *Renew Energy*. 2017;113:608-619.
 18. Xie L, Zhang X, Luo P, Huang P. Numerical study on the aerodynamic characteristics of both static and flapping wing with attachments. *J Phys: Conf Series*. 2017;916:012007.
 19. Wang X. Convective Heat Transfer and Experimental Icing Aerodynamics of Wind Turbine Blades. Ph. D thesis, University of Manitoba 2008.
 20. Alsabagh AS. *Effect of Atmospheric Ice Accretion on the Dynamic Performance of Wind Turbine Blades*. Hatfield, UK: University of Hertfordshire; 2016.
 21. Tarfaoui M, Shah OR. Spar shape optimization of a multi megawatts composite wind turbine blade: modal analysis. *Recent Adv Compos Mater Wind Turbine Blades*. Open Access - AMSA. 2013;Chapter 6, 93-104.
 22. Meng-Kao Yeh, Chen-Hsu Wang. Stress analysis of composite wind turbine blade by finite element method. IOP Conference Series: Materials Science and Engineering, Volume 241, 5th Asia Conference on Mechanical and Materials Engineering (ACMME 2017) 9–11 June 2017, Tokyo, Japan.
 23. Mishnaevsky L, Branner K, Petersen H, Beauson J, McGugan M, Sørensen B. Materials for wind turbine blades: an overview. *Materials*. 2017;10(11):1285.
 24. Tarfaoui M, Nachtane M, Khadimallah H, Saifaoui D. Simulation of mechanical behavior and damage of a large composite wind turbine blade under critical loads. *Appl Compos Mater*. 2017;25(2):237-254.
 25. Siemens. Siemens Global Website, 2008 [Online].
 26. Locke J, Valencia U, Ishikawa K. Design studies for twist-coupled wind turbine blades. *ASME 2003 wind energy symposium*. 2003;ASME 2003 wind energy symposium:324-331.
 27. Verelst D. Flexible wind turbine blades: a BEM-FEM coupled model approach. Delft University of Technology (TU Delft), 2009.
 28. Griffin DA. *Blade System Design Studies Volume I: Composite Technologies for Large Wind Turbine Blades*. SAND2002-1879. Albuquerque, NM: Sandia National Laboratories; 2002.
 29. Nachtane M, Tarfaoui M, Saifaoui D, El Moumen A, Hassoon OH, Benyahia H. Evaluation of durability of composite materials applied to renewable marine energy: case of ducted tidal turbine. *Energy Rep* 2018, (4), 31–40.
 30. Nachtane M, Tarfaoui M, Sassi S, El Moumen A, Saifaoui D. An investigation of hygrothermal aging effects on high strain rate behaviour of adhesively bonded composite joints. *Compos Part B Eng*. 2019;172:111-120.
 31. Jureczko M, Pawlak M, Mężyk A. Optimisation of wind turbine blades. *J Mater Process Technol*. 2005;167(2–3):463-471.
 32. Gemi L. Investigation of the effect of stacking sequence on low velocity impact response and damage formation in hybrid composite pipes under internal pressure. A comparative study. *Compos Part B Eng*. 2018;153:217-232.
 33. Tarfaoui M, Nachtane M, Boudounit H. Finite element analysis of composite offshore wind turbine blades under operating conditions. *J Therm Sci Eng Appl*. 2020;12:011001.
 34. Robynne EM, Roadman J, Beach R. Fusion joining of thermoplastic composite wind turbine blades: lap-shear bond characterization. *Renew Energy*. 2019;140:501-512.
 35. Boudounit H, Tarfaoui M, Saifaoui D. Structural Design and Analysis of a 5MW Offshore Wind Turbine Blades Under Critical Aerodynamic Loads. 14th Congress of Mechanics April 16–19, 2019 (Rabat, MOROCCO).
 36. Owaisur R. S. Identification and Characterization of the Mechanical and Structural Properties in Static Damage and Fatigue Resistance of a Composite Blade of a Floating Wind Turbine. Thesis / University of West Brittany, November 2014.
 37. Verma AS, Vedvik NP, Gao Z. Numerical assessment of wind turbine blade damage due to contact/impact with tower during installation. *IOP Conf Series: Mater Sci Eng*. 2017;276:12-25.
 38. Tarfaoui M, Shah OR, Nachtane M. Design and optimization of composite offshore wind turbine blades. *J Energy Resour Technol*. 2019;141:051204.
 39. Boudounit H, Tarfaoui M, Saifaoui D, Nachtane M. Structural analysis of offshore wind turbine blades using finite element method. *Wind Engineering*. 2019;44 168–180.
 40. Nachtane M, Tarfaoui M, El Moumen A, Saifaoui D. Damage prediction of horizontal axis marine current turbines under hydrodynamic, hydrostatic and impacts loads. *Compos Struct*. 2017;170:146-157.
 41. Lapczyk I, Hurtado JA. Progressive damage modeling in fiber-reinforced materials. *Compos A: Appl Sci Manuf*. 2007;38(11): 2333-2341.
 42. Soroush M, Fard KM, Shahravi M. Finite element simulation of interlaminar and intralaminar damage in laminated composite plates subjected to impact. *Latin Am J Solids Struct*. 2018;15 (6):e90.
 43. Tarfaoui M, Nachtane M, Shah OR, Boudounit H. Numerical study of the structural static and fatigue strength of wind turbine blades. *Materials Today: Proceedings*. 2019;13:1215-1223.
 44. Brøndsted P, Lilholt H, Lystrup A. Composite materials for wind power turbine blades. *Annu Rev Mat Res*. 2005;35(1): 505-538.
 45. Ghasemi A. R, Mohandes M. Composite Blades of Wind Turbine: Design, Stress Analysis, Aeroelasticity, and Fatigue. *Wind Turbines - Design, Control and Applications* 2016.
 46. Dai J, Hu W, Shen X. Load and dynamic characteristic analysis of wind turbine flexible blades. *J Mech Sci Technol*. 2017;31(4): 1569-1580.